

π -Expanded Ketocoumarins as Efficient, Biocompatible Initiators for Two-Photon-Induced Polymerization

Rashid Nazir,[†] Paulius Danilevicius,^{‡,#} Adina I. Ciuciu,[§] Maria Chatzinikolaidou,^{||} David Gray,[‡] Lucia Flamigni,^{*,§} Maria Farsari,^{*,‡} and Daniel T. Gryko^{*,†,⊥}

[†]Warsaw University of Technology Faculty of Chemistry, Noakowskiego 3, 00-664 Warsaw, Poland

[‡]Institute of Electronic Structure and Laser (IESL), Foundation for Research and Technology Hellas (FORTH), 711 10 Heraklion, Crete, Greece

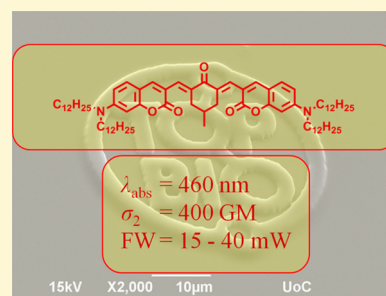
[§]Istituto per la Sintesi Organica e Fotoreattività (ISOF), CNR, Via Gobetti 101, 40129 Bologna, Italy

^{||}Department of Materials Science and Technology, University of Crete, Rethimno 741 00, Greece

[⊥]Institute of Organic Chemistry, Polish Academy of Sciences, Kasprzaka 44/52, Warsaw, Poland

Supporting Information

ABSTRACT: A series of π -expanded coumarins comprising of 4–5 conjugated rings were designed and synthesized. The strategic placement of two dialkylamino groups containing long alkyl chains attached to the peripheral ends of bis-coumarins resulted in dyes with superb solubility. As α,β -unsaturated ketones, these compounds display properties of donor–acceptor–donor (D–A–D)-type chromophores. Photophysical studies of the new functional dyes revealed a combination of favorable properties: strong absorption of blue and green light, weak fluorescence, reasonable two-photon absorption (2PA) cross-section, and complete solubility in nonpolar solvents. The fluorescence lifetimes of coumarin-derived α,β -unsaturated ketones were measured for the first time. The placement of two amine groups at peripheral positions of the dyes produced two-photon absorption cross-section values at the level of 150–400 GM around 800 nm, which generated two-photon photoinitiation. The highest 2PA cross-section was approximately 400 GM for the derivative of 4-methylcyclohexanone. Directly using these compounds as sensitizer or initiator, two (2D)- and three-dimensional (3D) nanopatterns were successfully fabricated by two-photon initiated polymerization. 3,3'-Carbonyl-biscoumarin, which contains two dihexylamino substituents at positions 7 and 7' possesses the largest fabrication window. MC3T3-E1 preosteoblastic cells exhibited strong adherence to all π -expanded coumarins and the same spindle-shaped morphology as the tissue culture treated polystyrene control surface. Additionally, our results showed an increase in cell proliferation after 3 and 7 days in culture, as well as a high cell viability of approximately 100% on all materials compared to the control surface. These findings confirm that D–A–D-type ketocoumarin derivatives used as potential photoinitiators are noncytotoxic and can be used in the fabrication of biomaterial scaffolds for tissue engineering applications.



INTRODUCTION

Two-photon-induced polymerization (TPIP) is a rapid prototyping technique utilized for the fabrication of small-scale, complex shaped three-dimensional (3D) objects, designed via computer-aided design (CAD). Since the first reported real 3D spiral microstructures,¹ by Maruo in 1997, the method has been investigated for various applications, such as photonic crystals,^{2,3} mechanical devices,^{4,5} and biomolecule scaffolds.⁶

While a large number of compounds possessing high two-photon absorption (2PA) cross-sections (σ_2) have been reported, the vast majority of them possess poor solubility combined with a low yield of radical generation.^{7–9} Consequently, pioneering researchers on two-photon polymerization^{10,11} used photoinitiators (PIs) designed for one-photon lithography in spite of the fact that the 2PA cross-section values were typically less than 40GM.¹² Trying to overcome these challenges, we have designed and efficiently synthesized a new

generation of photoinitiators possessing both a large σ_2 and high yield of radical photoinitiation.

The fundamental work of Fouassier and co-workers identified a range of efficient photoinitiators in classical free-radical polymerization.^{13–24} Both ketones^{25,26} as well as coumarins^{27–29} have been proven to possess such activity for many years. Although significant progress has occurred in the last years in photosensitizer design specifically tailored for 2PA,^{30–35} there are still remarkable challenges. One of them is 2PA initiators' solubility in monomers, which heavily affects their overall performance.³⁵ Our research focuses on applying α,β -unsaturated ketones being coumarin derivatives as a photosensitizer in TPIP by designing proper molecular systems, which enhance the σ_2 values. Since simple coumarins absorb

Received: February 19, 2014

Revised: April 17, 2014

Published: April 28, 2014

UV irradiation, typically this chromophore is π -extended in order to shift its absorption into the visible region (leading to high performance photosensitizers).³⁶

A limited number of studies have been conducted on the structure–property relationship of coumarin-based ketones. Of the limited coumarin derivatives prepared, very few have been used for photopolymerization.^{37,38} To our knowledge, there are no clear studies regarding the polymerization or burning thresholds. In this article we report the synthesis of several α,β -unsaturated ketone-based initiators for two-photon photopolymerization and investigate the effects of various side lengths as well as the influence of the central ketone ring size (Figure 1). In fact, the recent study by Liska and co-workers

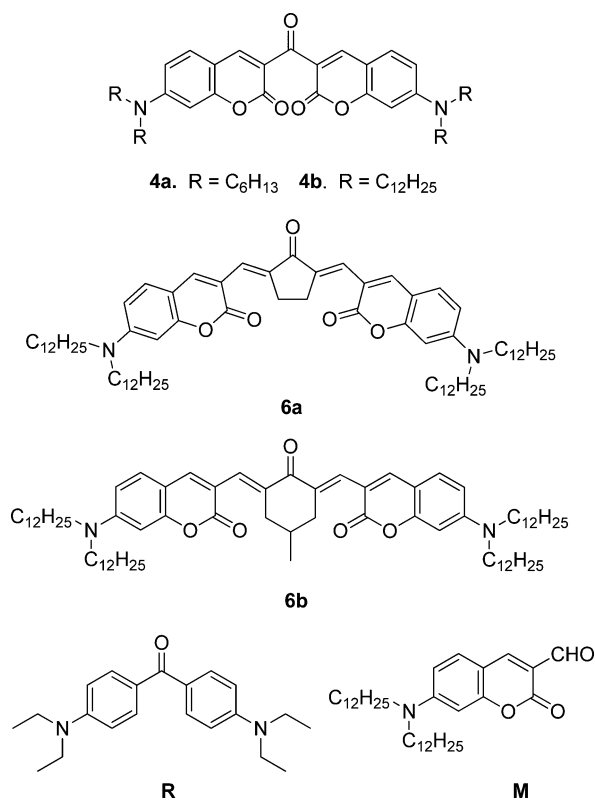


Figure 1. Structures of new 2PA PIs and reference compounds.

revealed that both photochemical and photophysical properties can be affected by the size of the central ring.³² Commercial availability of various cyclic ketones further justifies the importance of testing the effects of ring size on photochemical properties of α,β -unsaturated ketones. For comparison, the highly efficient 2PA PI **R** was also tested. An investigation of the photophysical properties of the initiators was conducted via UV–vis absorption and emission as well as z -scan measurements. Finally, TPIP structuring tests were performed at different laser intensities and feed rates to evaluate the 2PA initiation efficiency of each initiator. Understanding the interactions of materials chemistry with a specific cell type, exploration of cell attachment, viability, and proliferation on these materials is essential. In this study we examined the possible cytotoxicity of six different compounds when used as photoinitiators. The cellular response in terms of cell adhesion, viability, and proliferation on thin films of these materials was monitored after 1, 3, and 7 days in culture.

EXPERIMENTAL SECTION

Synthesis. All commercially available compounds were used as received. The typical details related to solvents, sorbents, and analyses are described in detail in the Supporting Information. *N,N*-Dialkylaminophenols **2a–b** were obtained by the reported method,³⁹ and their physical properties concurred with the published data.⁴⁰

General Procedure for Synthesis of 4-(Dialkylamino)-2-hydroxybenzaldehydes. Anhydrous dimethylformamide (DMF) (8.8 g, 120 mmol) was cooled in an ice–water bath, and then phosphorus oxychloride (2.0 mL, 20 mmol) was added dropwise with stirring by heating at 40 °C for 30 min. A bright yellow Vilsmeier–Haack reagent resulted and was cooled again in an ice–water bath. 3-(Dialkylamino)-phenol (17 mmol) was added dropwise. After stirring for 30 min, the mixture was heated at 70 °C for 6 h. Then the mixture was cooled and poured into ice water. The product was extracted from water with ethyl acetate. The organic layer was washed with a saturated solution of sodium bicarbonate (aqueous solution, 100 mL). The organic phase was dried over MgSO₄ and evaporated in vacuum.

4-(Dihexylamino)-2-hydroxybenzaldehyde (3a). The crude product was purified by chromatography on silica gel (eluent, ethyl acetate; hexanes, 20:1) as a light yellow oil with yield 69%. ¹H NMR (200 MHz, CDCl₃): δ 11.65 (s, 1H), 9.47 (s, 1H), 7.28–7.22 (d, J = 8.8 Hz, 1H), 6.25–6.19 (dd, J_1 = 2.2 Hz, J_2 = 2.4 Hz, 1H), 6.03–6.02 (d, J = 2.4 Hz, 1H), 3.33–3.26 (t, J = 15.6 Hz, 4H), 1.62–1.59 (m, 4H), 1.33–1.26 (m, 12H), 0.90–0.84 (t, J = 13 Hz, 6H). ¹³C NMR (200 MHz, CDCl₃) δ 191.9, 164.4, 154.7, 153.4, 111.4, 104.6, 96.9, 51.36, 32.0, 29.7, 29.5, 29.4, 27.4, 27.1, 22.8, 22.4, 14.2. HRMS (ESI): m/z ([M + H]⁺) C₁₉H₃₁NO₂, calculated 305.2355; found 305.2367.

4-(Didodecylamino)-2-hydroxybenzaldehyde (3b). Purification was done by chromatography on silica gel (eluent, ethyl acetate; hexane, 30:1) as a light yellow oil with yield 56%. ¹H NMR (200 MHz, CDCl₃): δ 11.65 (s, 1H), 9.47 (s, 1H), 7.22 (s, 1H), 6.25–6.19 (dd, J_1 = 2.2 Hz, J_2 = 2.4 Hz, 2H), 6.03–6.02 (d, J = 2.4 Hz), 3.36–3.25 (t, J = 2.5 Hz, 4H), 1.62–1.59 (m, 4H), 1.33–1.26 (m, 36H), 0.90–0.84 (t, J = 11.5 Hz, 6H). ¹³C NMR (200 MHz, CDCl₃) δ 191.6, 164.4, 154.7, 135.3, 111.4, 104.6, 96.97, 96.90, 51.3, 32.0, 30.6, 29.7, 29.58, 29.50, 27.4, 27.1, 22.8, 14.2. HRMS (ESI): m/z ([M + H]⁺) C₃₁H₅₆NO₂, calculated 474.4317; found 474.4311.

General Procedure for Synthesis of Ketocoumarins. The salicylaldehyde (2 mmol) and dimethyl 1,3-acetonedicarboxylate (1 mmol) were dissolved in 10 mL of ethanol. Piperidine (10–20 drops) was added, and the mixture was heated at reflux for 2 h. The mixture was cooled down to room temperature, and subsequently, the solvent was evaporated.

3,3'-Carbonylbis(7-(dihexylamino)-2H-chromen-2-one) (4a). The crude product was purified by recrystallization with ethanol as a orange solid with yield 79%. ¹H NMR (500 MHz, CDCl₃): δ 8.15 (s, 2H), 7.36–7.35 (d, J = 9 Hz, 2H), 6.56–6.54 (dd, J_1 = 2.5 Hz, J_2 = 2.5 Hz, 2H), 6.45 (s, 2H), 3.33–3.31 (t, J = 15.5, 8H), 1.61–1.58 (m, 8H), 1.33–1.27 (m, 24H), 0.92–0.89 (t, J = 13 Hz, 12H). ¹³C NMR (500 MHz, CDCl₃) δ 188.7, 160.5, 158.2, 152.7, 145.9, 131.1, 120.3, 109.6, 108.5, 97.4, 51.6, 31.7, 27.3, 26.8, 22.7, 14.1. HRMS (ESI): m/z ([M + H]⁺) C₄₃H₆₁N₂O₅; calculated 685.4580; found 685.4586.

3,3'-Carbonylbis(7-(didodecylamino)-2H-chromen-2-one) (4b). The crude product was purified by recrystallization with ethanol as an orange solid with yield 49%. ¹H NMR (500 MHz, CDCl₃): δ 8.15 (s, 2H), 7.36–7.34 (d, J = 9 Hz, 2H), 6.56–6.54 (dd, J_1 = 2 Hz, J_2 = 2.5 Hz, 2H), 6.45 (s, 2H), 3.34–3.31 (t, J = 15.8H), 1.61–1.56 (m, 8H), 1.33–1.26 (m, 72H), 0.89–0.86 (t, J = 13.5 Hz, 12H). ¹³C NMR (500 MHz, CDCl₃) δ 188.7, 160.5, 158.2, 152.8, 145.9, 131.1, 120.3, 109.6, 108.5, 97.4, 51.6, 32.0, 29.8, 29.76, 29.75, 29.71, 29.58, 29.47, 27.36, 27.1, 22.8, 14.2. HRMS (ESI): m/z ([M + H]⁺) C₆₇H₁₀₈N₂O₅Na; calculated 1043.8146; found 1043.8129.

7-(Didodecylamino)-2H-chromen-2-one (5). 4-(Didodecylamino)-2-hydroxybenzaldehyde (2.36 g, 5 mmol), diethylmalonate (1.6 g, 10 mmol), and piperidine (1 mL) were combined in absolute ethanol (30 mL) and stirred for 6 h under reflux conditions. Ethanol was evaporated under reduced pressure, then concentrated HCl (20 mL)

and glacial acetic acid (20 mL) were added to hydrolyze the reaction with stirring for another 6 h. The solution was cooled to room temperature and poured into 100 mL of ice water. NaOH solution (40%) was added dropwise to modulate the pH of the solution to ~5, extracted with ethyl acetate (3 times), and washed with 10 mL saturated NaHCO₃ followed by 10 mL of water. The organic phase was dried (MgSO₄) and solvent removed by rotary evaporation. The crude product was used as such without any further purification to synthesize aldehyde **M**.

7-(Didodecylamino)-2-oxo-2H-chromene-3-carbaldehyde (M). Anhydrous DMF (8.8 g, 120 mmol) was cooled in an ice–water bath, and then phosphorus oxychloride (2 mL, 20 mmol) was added dropwise with stirring and then heated at 40 °C for 30 min. A bright yellow Vilsmeier–Haack reagent was formed and cooled again in an ice–water bath, and **5** (6 mmol) was added dropwise to the Vilsmeier–Haack reagent. After stirring for 30 min, the mixture was heated at 70 °C for 6 h. Then the mixture was cooled and poured into ice water. The product was extracted from water with ethyl acetate. The organic portion was washed with a saturated solution of sodium bicarbonate NaHCO₃ aqueous solution (100 mL) to remove any remaining acid in the ethyl acetate. The organic phase was dried over MgSO₄ and evaporated under vacuum. The crude product was purified by recrystallization with absolute ethanol to give yellow solid with yield 67%. ¹H NMR (500 MHz, CDCl₃): δ 10.12 (s, 1H), 8.24 (s, 1H), 7.40–7.38 (d, *J* = 9.5 Hz, 1H), 6.60–6.58 (dd, *J*₁ = 2, *J*₂ = 2.5, 1H), 6.45 (s, 1H), 3.37–3.34 (t, *J* = 15.5 Hz, 4H), 1.62 (m, 4H), 1.33–1.22 (m, 36H), 0.89–0.86 (t, *J* = 13.5 Hz, 6H). ¹³C NMR (500 MHz, CDCl₃) δ 188.0, 162.1, 159.0, 153.9, 145.4, 132.5, 114.3, 110.4, 108.3, 97.4, 51.7, 32.0, 29.76, 29.75, 29.71, 29.68, 29.55, 29.47, 29.3, 27.1, 22.8, 14.2. HRMS (ESI): *m/z* ([M + Na]⁺) calcd for C₃₄H₅₅NO₃Na: calculated 548.4089; found 548.4080.

General Synthesis Procedure for Cyclic Benzylidene Ketones 6a and 6b. The following reagents were added to toluene (10 mL): aldehyde **M** (2 mmol), corresponding cyclic ketone (1 mmol), piperidine (85 mg), and glacial acetic acid (60 mg). The solution was refluxed for 1 h and another 85 mg of piperidine and 60 mg of acetic acid were added. After refluxing for an additional 30 min, the reaction mixture was cooled, diluted with 50 mL of Et₂O, and washed with 10 mL saturated NaHCO₃ followed by 10 mL of water. The organic phase was dried (MgSO₄) and the solvent removed by rotary evaporation.

3,3'-(1E,1'E)-(2-Oxocyclopentane-1,3-diyldene)bis(methan-1-yl-1-ylidene)bis(7-(didodecylamino)-2H-chromen-2-one) (6a). The crude product was purified by recrystallization with *n*-pentane as a red solid with yield 48%. ¹H NMR (500 MHz, CDCl₃): δ 7.75 (s, 2H), 7.72 (s, 2H), 7.31–7.29 (d, *J* = 10 Hz, 2H), 6.60–6.55 (dd, *J*₁ = 5 Hz, *J*₂ = 5 Hz, 2H), 6.42 (d, *J* = 2.1 Hz, 2H), 3.35–3.31 (t, *J* = 10 Hz, 8H), 3.03 (s, 4H), 1.62 (m, 8H), 1.34–1.28 (m, 72H), 0.90–0.88 (m, 12H). ¹³C NMR (500 MHz, CDCl₃) δ 194.1, 161.5, 156.4, 151.7, 142.1, 137.7, 128.8, 127.1, 116.7, 109.5, 108.5, 99.9, 97.3, 51.4, 31.9, 29.65, 29.60, 29.3, 29.60, 29.56, 29.45, 29.32, 27.17, 27.03, 22.66, 22.7, 14.1. HRMS (FD): *m/z* ([M]⁺) calcd for C₇₃H₁₁₄N₂O₅: calculated 1098.87; found 1098.91.

3,3'-(1E,1'E)-(5-Methyl-2-oxocyclohexane-1,3-diyldene)bis(methan-1-yl-1-ylidene)bis(7-(didodecylamino)-2H-chromen-2-one) (6b). The crude product was purified by recrystallization with *n*-pentane as a red solid with yield 41%. ¹H NMR (500 MHz, CDCl₃): δ 7.74 (s, 2H), 7.52 (s, 2H), 7.27–7.29 (d, *J* = 10 Hz, 2H), 6.55–6.54 (d, *J* = 5 Hz, 2H), 6.38 (s, 2H), 3.30–3.28 (t, *J* = 12.5, 8H), 2.90–2.88 (m, 2H), 2.46–2.41 (m, 2H), 1.59 (m, 8H), 1.32–1.26 (m, 72H), 1.08–1.07 (m, 3H), 0.89–0.87 (m, 12H). ¹³C NMR (500 MHz, CDCl₃) δ 187.8, 161.4, 156.2, 151.3, 147.5, 136.2, 130.9, 129.5, 116.4, 109.2, 108.4, 97.33, 97.31, 51.3, 37.1, 31.8, 29.62, 29.61, 29.60, 29.56, 29.45, 29.32, 27.17, 27.03, 22.66, 21.6, 14.0. HRMS (ESI): *m/z* ([M + H]⁺) calcd for C₇₅H₁₁₈N₂O₅: calculated 1126.90; found 1127.91.

Resin Preparation. All the chemicals used in this work were obtained from commercial sources and used without further purification.

In the final resin, methacryloxypropyl trimethoxysilane (MAPTMS) and methacrylic acid (MAA) were used as the organic photo-

polymerizable monomers. The additional ingredients, i.e., ZPO (zirconium propoxide, 70% in propanol), the alkoxy silane groups of MAPTMS, served as the inorganic network forming moieties. The preparation of monomer used in two-photon polymerization was described earlier.⁴¹

In the first step MAPTMS was suspended in HCl solution (0.1 M) at 1:0.1 ratio, which induced its hydrolysis. In parallel, MAA was added to ZPO (molar ratio 1:1) as a stabilizing agent. Subsequently, to the hydrolyzed MAPTMS, the zirconium complex was slowly added at a 2:8 molar ratio. The given photoinitiator (at 1% w/w concentration) was added as a last one to the mixture. Following stirring for 15 min, the composite was filtered using a 0.22 μm syringe filter.

In the next phase, the heating process led to the condensation of alkoxide groups and the formation of the inorganic matrix. Specifically, the samples were prepared by drop-casting onto 100 μm thick silanized glass substrates, followed by drying the resultant films for 10 min in an oven at 80 °C. Subsequently, the organic moieties attached to the inorganic backbone were polymerized using TPPI.

Photophysics. Spectroscopic grade toluene and dichloromethane (C. Erba) and ethyl iodide (Aldrich) were used. All experiments were run on freshly prepared solutions. Absorption spectra were recorded with a PerkinElmer Lambda 9 spectrophotometer. Emission spectra were collected by an Edinburgh FLSP920 fluorimeter equipped with a R928P Hamamatsu photomultiplier and corrected for the photomultiplier (PMT) response if not otherwise stated. Corrected phosphorescence spectra and lifetimes were measured on the same Edinburgh FLSP920 apparatus, equipped with a microsecond XeμF920H flash lamp. Delayed spectra were registered with a gate of 10 ms and a delay, with respect to the excitation, of 0.5 ms. Air equilibrated solutions in standard 10 mm quartz cells were used for experiments at room temperature, whereas luminescence determination at 77 K was performed on quartz tubes dipped in liquid nitrogen in a quartz Dewar. Luminescence quantum yields of the samples, ϕ_s were evaluated at room temperature against a standard with known emission quantum yield ϕ_r . The areas under the corrected luminescence spectra were compared by using the equation: $\phi_s/\phi_r = A_r n_s^2(\text{area})_s/A_s n_r^2(\text{area})_r$, where *A* is the absorbance, *n* is the refractive index of the solvent employed, and *s* and *r* represent the sample and reference, respectively. The standard used was air-equilibrated Coumarin 153 in ethanol, yield $\phi_R = 0.544$.⁴²

Fluorescence lifetimes in the nanosecond region were detected by a Time Correlated Single Photon Counting apparatus (IBH) with excitation at 465 nm and a time resolution of ca. 0.5 ns. In order to measure fluorescence lifetimes in the picosecond region, a Streak Camera Hamamatsu C1587 equipped with M1952 was used as detector after excitation with a Nd:YAG laser at 355 nm (Continuum PY62/10, 35 ps pulse, 1 mJ).⁴³ Estimated errors on photophysical determinations are 10% for lifetimes and 20% for molar extinction coefficients and quantum yields. The working temperature was 295 ± 2 K, if not otherwise specified.

z-Scan Technique. The experimental setup to measure two-photon absorption cross-sections using Z-scan technique was described earlier⁴⁴ (see Supporting Information for details).

Fabrication of Microstructures with DLW Setup. The experimental setup used for the DLW of the 3D structures has been described previously.⁴⁵ A Ti:sapphire femtosecond laser (Femtolasers Fusion, 800 nm, 75 MHz, <20 fs) was tightly focused into the volume of the photosensitive hybrid material using a high numerical aperture microscope objective lens (100×, N.A. = 1.4, Zeiss, Plan Apochromat). Sample movement in the *xyz* space was achieved using piezoelectric stages (PhysikInstrumente). The DLW procedure was controlled through a computer using the 3DPoli software. The average laser power was measured before the objective, and the scanning velocity was 200 μm/s. After the completion of the fabrication process, the samples were developed for 20 min in 4-methyl-2-pentanone.

2PA Cross-Section Measurements. In order to investigate 2PA properties of the compounds, the z-scan technique was used. The z-scan technique is based on the measurement of the transmittance when a focused laser beam passes through a sample of nonlinear

media. The sample is translated along the axis of the focused beam. When approaching the waist of the beam, the intensity is at a maximum. If the nonlinear absorption threshold is exceeded and the sample exhibits multiphoton absorption, a decrease in the light transmittance can be observed, depending on the sample position with respect to the beam waist. By fitting the transmittance versus the sample position (Figure 5), the multiphoton absorption cross-section can be extracted. If the dominant process is two-photon absorption, the z -scan transmittance can be expressed as

$$T(z) = \sum_{n=0}^{\infty} \frac{(-q_0)^n}{(n+1)^{3/2} (1+x^2)^n}$$

where $q_0 = I_0 L_{\text{eff}} N_A \rho \times 10^{-3} \sigma_2 \lambda / hc$, I_0 is the laser intensity at the beam waist, which is calculated as $I_0 = 2E/\pi^{3/2} \tau w_0^2$, E is the laser pulse energy, τ is the pulse duration, w_0 is the beam waist radius, L_{eff} is the effective sample thickness, which is expressed as $L_{\text{eff}} = (1 - e^{-\alpha L})/\alpha$, α is the single-photon absorption coefficient, L is the sample thickness, N_A is the Avogadro constant, ρ is the concentration of the sample in mol/L, λ is the wavelength of the laser, h is the Planck constant, c is the speed of light, σ_2 is the two-photon absorption cross-section, $x = z/z_0$, z is sample position, and z_0 is the Rayleigh length.

Materials Film Preparation for the Cytotoxicity Assays. For the investigation of cell adhesion and cell proliferation quantification we prepared thin films by depositing the different materials on round glass substrates (coverslips) using the spin-coating technique. One hundred microliters of a photopolymer solution doped with the different initiators were placed on 100 μm thick coverslips with a diameter of 15 mm and spin-coated with a speed of 1500 rpm for 120 s to obtain thin films. The employed photoinitiator concentrations were (i) 1 wt % of the commercial standard initiator (bisIp), (ii) 5 mM commercial standard initiator, which corresponds to 0.16 wt % (bisSm), (iii) 5 mM custom synthesized initiator **4b**, (iv) 5 mM custom synthesized initiator **6a**, (v) 5 mM custom synthesized initiator **6b**, and (vi) 5 mM custom synthesized initiator **4a**. The films were dried in an oven at 40 $^{\circ}\text{C}$ for 2 h to evaporate the solvent. Then they were photopolymerized using a KrF excimer laser working at 248 nm wavelength resulting in the formation of even films as observed by scanning electron microscopy (SEM) (data not shown).

Cell Culture. Cell culture media and reagents were purchased from Invitrogen (Life Technologies). Preosteoblastic MC3T3-E1 cells (DSMZ GmbH, Braunschweig, Germany) between passages 7 and 10 were maintained and expanded in α -MEM, supplemented with glutamine (2 mM), penicillin (50 IU/mL), streptomycin (50 g/mL), and 10 vol % FBS in a humidified atmosphere at 37 $^{\circ}\text{C}$ and 5% CO_2 in a cell culture incubator. Confluent cells were passaged after trypsination (0.25% trypsin in 1 mM EDTA), seeded at 60–80% confluence and cultured in flasks by replacing fresh medium every 2 days for the entire duration of the experiments.

Cell Adhesion on Different Material Samples. For examining cell adhesion and morphology on the various material films, the samples were first sterilized with 70% ethanol, air-dried under the laminar flow, and rinsed briefly with culture medium. Each sample was placed in a single well of a 24-well plate and seeded with 2×10^4 cells per sample. After 1, 3, and 7 days in culture, the samples were rinsed with phosphate buffer saline and imaged by means of a Zeiss Axiovert 200 microscope. Images were taken by a ProgResCFscanJenoptik camera (Jena, Germany) using the ProgResCapturePro 2.0 software and an objective lens for 10-fold magnification.

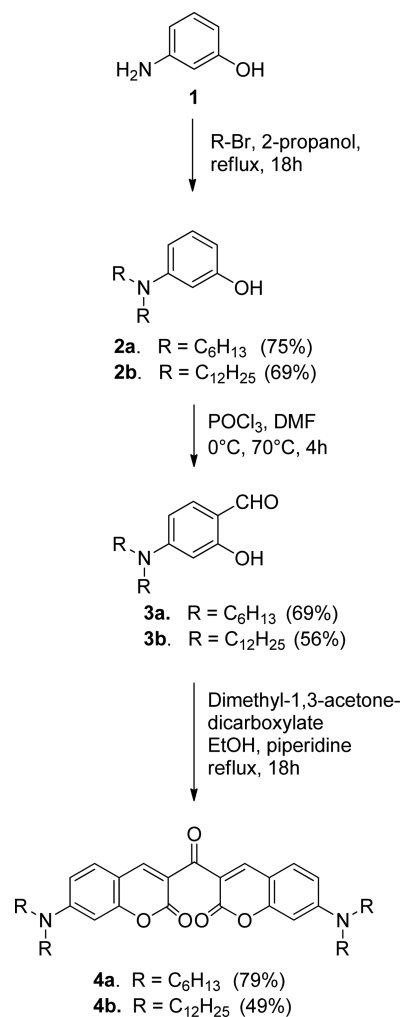
Cell Viability and Proliferation Assay. For the investigation of cell viability and proliferation on the various material films, the samples were first sterilized with 70% ethanol, then air-dried under a laminar flow and rinsed briefly with culture medium. Each one was placed in a single well of a 24-well plate and seeded with 5×10^4 cells per sample. On days 1, 3, and 7 postseeding, cell viability and proliferation assays were performed using the resazurin-based PrestoBlue reagent according to the manufacturer's instructions. The cells were incubated with the reagent for 60 min at 37 $^{\circ}\text{C}$. The optical density was measured in a spectrophotometer (Molecular Devices SpectraMax M2), and cell number quantification was performed by means of a

calibration curve.⁴⁶ Error bars represent the average of triplicates \pm standard deviation.

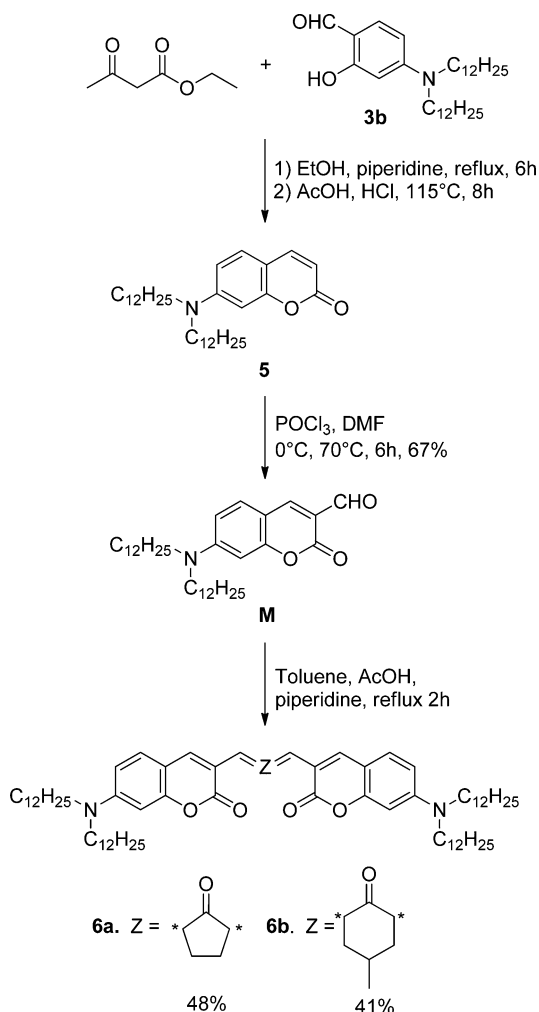
RESULTS AND DISCUSSION

We designed two types of coumarin-based photoinitiators (Schemes 1 and 2). 3,3-Carbonyl-biscoumarin bearing strongly

Scheme 1. Synthesis of Keto-biscoumarins 4a and 4b



electron-donating diethylamino groups has been thoroughly studied as a photoinitiator in classical photopolymerization.²⁹ As a photoinitiator, it displays favorable properties such as high yield of intersystem crossing, but when applied to 2PA systems, it lacks critical features such as solubility within commercial monomers. Therefore, we devised an advanced design, which improves solubility by attaching long alkyl chains on the amine nitrogen substituent. We reasoned that this structural change will not significantly influence the optical properties while appreciably improving solubility in nonpolar solvents. The synthesis followed the general route toward this type of bis-ketocoumarin, first reported by Specht et al.²⁹ 3-Aminophenol (**1**) was alkylated on nitrogen with 1-bromohexane and 1-bromododecane, followed by Vilsmeier–Haack formylation of phenols **2a** and **2b** (Scheme 1). Resulting aldehydes **3a** and **3b** were subsequently transformed into π -expanded bis-coumarins **4a** and **4b** by Knoevenagel condensations with dimethyl acetone-1,3-dicarboxylate (Scheme 1). Encouraged by several reports describing favorable performance of α,β -unsaturated

Scheme 2. Synthesis of Bis-coumarins **6a** and **6b**

ketones in TPIP^{29,37} we resolved to transform aldehyde **3b** into formyl-coumarin **M** and subjected it to double aldol condensation with cyclopentanone and 4-methylcyclohexanone producing compounds **6a** and **6b** with a reasonable overall yield (Scheme 2). As catalysts for aldol reaction of this type, both strong bases or acids⁴⁷ as well as complexes of metal (II) ions can be used.^{48,49} Synthesis of **6a** and **6b** has been achieved by using piperidinium acetate as a catalyst with moderate yields. They represent one of the largest π -conjugated systems containing coumarins synthesized to date. As predicted, all four dyes displayed superb solubility in a wide range of solvents including hexane. The purity and identity of all new compounds (**3a,b**, **4a,b**, **M**, and **6a,b**) was unequivocally confirmed using ¹H NMR, ¹³C NMR, and high-resolution mass spectrometry.

Optical Properties and Photophysics. Experiments were conducted in two solvents of different polarity, toluene (TOL) with dielectric constant, $\epsilon = 2.38$, and dichloromethane (DCM), $\epsilon = 8.93$. The absorption spectra in the two solvents are collected in Figure S1, Supporting Information, and the derived parameters are collected in Table 1.

The absorption spectra of **4a** and **4b** are almost identical with a sharp absorption maximum at 450 nm and with an epsilon value close to 100 000 M⁻¹ cm⁻¹. The spectral features are not dissimilar from the ones of the aldehyde **M**, though; in the latter, the maximum is 10 nm hypsochromically shifted and the

Table 1. Spectroscopic and Photophysical Parameters of the Samples at Room Temperature

	ϵ (M ⁻¹ cm ⁻¹) ($\lambda_{\text{abs}}^{\text{max}}$ (nm))	$\lambda_{\text{em}}^{\text{max}}$ (nm)	Δ_{ss} (cm ⁻¹)	ϕ_{fl}	τ (ns)	k_{rad} (sec ⁻¹)
TOL						
4a	89700 (451)	477	1210	0.010	0.05 (80%) 0.16 (20%)	2.0×10^8
4b	91000 (450)	475	1170	0.010	0.05 (80%) 0.16 (20%)	2.0×10^8
6a	55100 (479); 57900 (504)	540; 578 (sh)	1320	0.251	0.900	2.8×10^8
6b	72100 (460)	514; 558 (sh)	2280	0.025	0.07	3.6×10^8
M	52700 (440)	462	1080	0.576	1.95	2.9×10^8
DCM						
4a	91400 (464)	506	1790	0.003	0.01 (85%) 0.17 (15%)	3.0×10^8
4b	93700 (464)	504	1710	0.003	0.02 (85%) 0.19 (15%)	1.5×10^8
6a	64100 (523)	605	2590	0.313	1.2	2.6×10^8
6b	75800 (485)	582	3440	0.078	0.27	2.9×10^8
M	56200 (450)	483	1520	0.656	2.47	2.6×10^8

molar absorption coefficient is almost half. The other two compounds **6a** and **6b** show largely bathochromically shifted broader spectra ($\epsilon = 60\,000$ – $80\,000$ M⁻¹ cm⁻¹) in comparison to **M**, indicative of an extended conjugation. A weak vibronic structure is also evident in **6a**. The absorption spectra of all samples shift bathochromically in the more polar DCM, from 10 nm in the aldehyde **M** to 25 nm in the more π -extended compounds **6a** and **6b**. One can also notice that the weak vibronic structure present in TOL solutions of **6a** tends to disappear in DCM. The bathochromic shift is indicative of a transition that occurs at lower energy in the polar solvent. This might be due either to a destabilization of the ground state or to a stabilization of the excited state in the vertical transition.

The room temperature fluorescence spectra from optically matched solutions are reported in Figure 2. The aldehyde **M** displays a high fluorescence quantum yield (0.576 in TOL and 0.656 in DCM). The spectral features and the fluorescence quantum yields (ϕ_{fl}) of **4a** and **4b** are almost identical, only slightly bathochromically shifted with respect to those of the aldehyde **M**, but with a much lower fluorescence quantum yield compared to that of **M**. They in fact display a ϕ_{fl} of the order of a few percent in both TOL and DCM. Sample **6b** has a ϕ_{fl} slightly higher than that of the former samples, of the order of 5–10% of that of **M**, whereas the compound **6a** has a noticeable luminescence, of the order of 50% of that of the reference aldehyde **M**. The trend of ϕ_{fl} within the series is similar in both solvents, with a higher luminescence quantum yield in DCM compared to TOL for **6a**, **6b**, and **M**, whereas **4a** and **b** have a lower ϕ_{fl} in DCM. One can notice that the Stokes shift (Δ_{ss}) are in general higher in DCM than in TOL, but from a qualitative viewpoint, Δ_{ss} for the various samples in TOL parallel the one in DCM, with a larger Stokes shifted emission for sample **6a** and even more for **6b**. For the latter, a value of ca. 2200 and 3400 cm⁻¹ is detected in TOL and DCM,

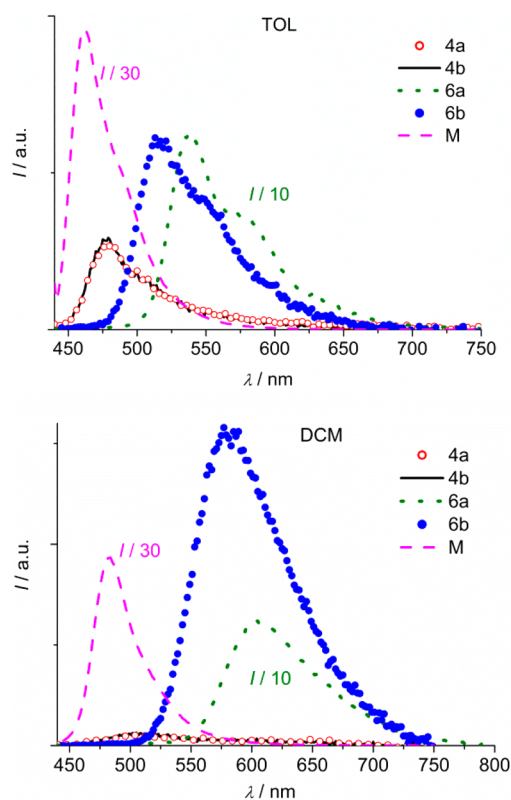


Figure 2. Room temperature corrected luminescence spectra in TOL and DCM; λ_{exc} is 440 nm and $A_{440\text{nm}} = 0.10$ for all samples.

respectively. These values testify to the large change in polarity from the ground to the relaxed excited state. An increased charge transfer character in the excited state is compatible with the observations. Accordingly, as observed for the absorption features a vibronic structure present in the emission spectra of **6a** and **6b** in TOL solutions is lost in DCM. The luminescence data are collected in Table 1. The reported data are in good agreement with former reports on similar samples.^{29,36}

The excitation spectra of the samples registered on the emission maxima return the absorption spectra, indicating a genuine nature of the emission and the purity of the sample (Figure S2, Supporting Information).

The data on lifetimes are missing in the literature also for the already published ketocoumarins due to the subnanosecond lifetime of the bis-ketocoumarin derivatives, which require nonstandard time-resolved luminescence techniques. In addition to a time-correlated single-photon counting

(TCSPC) apparatus, we used a streak camera equipment with 10 ps resolution. This technique allowed to measure the luminescence lifetime of all samples, reported in Table 1; a couple of examples are shown in Figure 3. At variance with the cases of samples **6a**, **6b**, and **M**, which have a strict exponential decay lifetime, the 3,3'-bis-coumarins **4a** and **4b** display a biexponential decay in both solvents, with a major component with a tens of picoseconds lifetime and a 15%–20% component with about a two hundred picosecond lifetime. The presence of a double exponential, ascribable to two different types of populations in the excited state, has been formerly reported for a similar compound and ascribed to the presence of different conformers.⁵⁰ Whereas the aldehyde lifetime is in the nanosecond range, the bis-coumarin samples display lifetimes of the order of tens/hundreds of picoseconds. The lifetimes in DCM solutions are higher than those in TOL for samples **6a**, **6b**, and **M**, whereas they are slightly lower for samples **4a** and **4b**. This parallels the trend of luminescence quantum yield; in fact, the calculated radiative rate constants $k_{\text{rad}} = \phi_{\text{fl}}/\tau$ are, for all samples, almost unaffected by solvent polarity, within experimental error.⁵¹ This, in broad terms, indicates that the triplet yield (ϕ_{isc}), whose formation occurs from the lowest singlet excited state in competition with the radiative deactivation, should also be unaffected by the solvent. From the polymerization viewpoint, the formation of a high triplet yield is crucial. The maximum achievable triplet yield (maTY) is the difference between unity and the emission quantum yield. From this simplified approach, the lower maTY can be derived for sample **6a**, which has the highest emission quantum yield, $\phi_{\text{fl}} = 0.25$ and 0.31 in TOL and DCM, respectively. Photopolymerization is a very complex process and even more is 2PA photopolymerization, so the number of parameters affecting the process is quite large. However, as formerly pointed out,²⁹ the luminescence properties and hence the triplet yield formation can give a broad indication.

As a final step in the characterization of the lowest excited states of the samples, we determined the luminescence properties at 77 K in a rigid TOL glass. This determination provides a precise E_{00} value for the singlet excited level, for which we conventionally assume the energy of the emission maxima at 77 K, and it can provide the triplet energy level from the phosphorescence spectra. In Table 2 the results of the luminescence experiments at 77 K are summarized. In samples **4a** and **4b** a high triplet quantum yield is expected, based on the literature data ($\phi_{\text{isc}} = 0.92$)²⁹ for very similar samples. In fact, the phosphorescence can be easily detected in the prompt luminescence spectra and can be isolated from fluorescence by

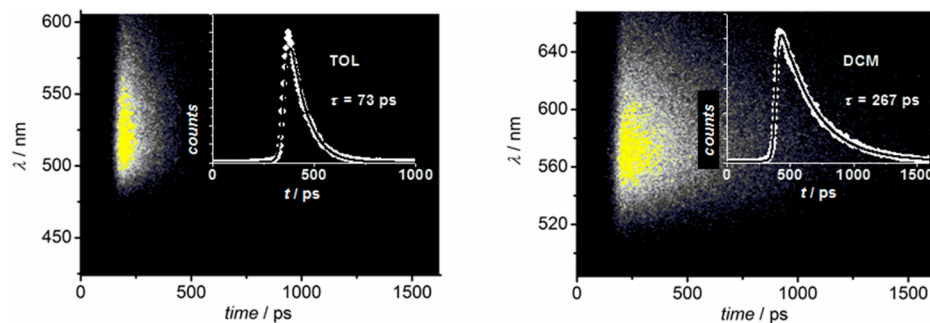


Figure 3. Streak camera images of compound **6b** in TOL and DCM. The time decays registered on the emission maxima with the exponential fitting are shown.

Table 2. Band Maxima and Energies of Fluorescence and Phosphorescence in TOL Solid Matrix at 77 K

77 K			
	state	$\lambda_{\text{em}}^{\text{max}}$ (nm)	E (eV)
4a	¹ 4a	482	2.57
	³ 4a	560; 609	2.21
4b	¹ 4b	482	2.57
	³ 4b	559; 607	2.21
6a	¹ 6a	494; 545	2.51
	³ 6a	587; 625	2.11
6b	¹ 6b	493; 529	2.51
	³ 6b	587; 629	2.11
M ^a	¹ M	462; 494	2.68
	³ M	578; 631	2.14

^aSolvent is TOL/EtI (1:1).

gating the signal (see experimental section for details), Figure S3, Supporting Information. Similarly, the phosphorescence of samples **6a** and **6b** can be detected in TOL glasses, whereas for aldehyde **M** the use of a heavy atom solvent as ethyl iodide (EtI) is required. The presence of the latter increases the spin-orbit coupling and hence the triplet yield and allows detection of the spectral features of the phosphorescence in the aldehyde **M**, which is characterized by a high luminescence quantum yield and hence by a low ϕ_{isc} . Figure 4 reports some examples of the fluorescence (prompt luminescence) and phosphorescence (delayed luminescence) spectra detected at 77 K. The measured phosphorescence lifetime is 25 ± 3 ms for all samples.

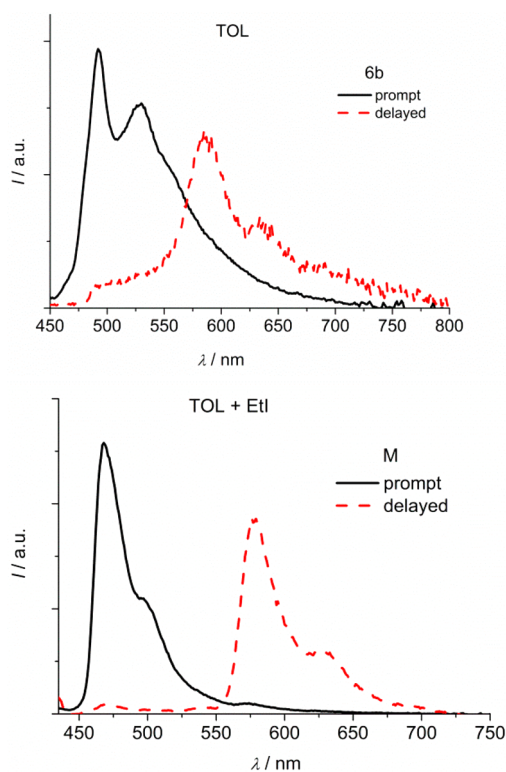


Figure 4. Arbitrarily scaled prompt and delayed (see experimental section for details) luminescence measured in glassy solutions at 77 K for **6b** in TOL and for **M** in TOL/EtI. Excitation at 430 nm.

The singlet–triplet splitting is of the order of 0.3–0.4 eV in samples **4** and **6** and increases to 0.54 eV in aldehyde **M**. A larger splitting is generally associated with a less efficient intersystem crossing, and apparently this is the case here.

2PA measurements were repeated with several different laser intensities in order to calculate average cross-section values. From results in Table 3 it can be seen that compound **6b**

Table 3. 2PA Cross-Section Values of the Compounds Measured by z-Scan at 800 nm

compd	solvent	concentration (mol/L)	σ_2 (GM)
4a	DCM	0.01	150.0 ± 3.0
4b	DCM	0.01	90.0 ± 1.8
6a	DCM	0.01	60.0 ± 1.2
6b	DCM	0.01	401.0 ± 8.0
R	1-propanol	0.25	6.0 ± 0.1

exhibits the highest 2PA cross-section. All the synthesized compounds exhibit 1 order of magnitude higher 2PA cross-section than the reference compound (Figure 5).

Fabrication Properties. The one-photon capability of the synthesized photoinitiators was confirmed by polymerizing drop-cast films of the material using a wide-spectrum UV lamp.

In order to investigate the efficiency of synthesized TPIP photoinitiators the sample grid structures were fabricated using a direct laser writing (DLW) setup. There are three characteristic parameters that can be used to describe the fabrication process qualitatively. These are (a) polymerization threshold, the minimal laser power that ensures that fabricated structures can survive the development stage; however, structures tend to have deformations due to low polymerization degree at the threshold power; (b) good structuring threshold, structures fabricated with higher power than this threshold have a good quality; (c) burning threshold, the level of laser power at which good quality fabrication can no longer be achieved due to the microexplosions that occur during materials processing from optical damage. Typical microstructures fabricated under these threshold conditions are demonstrated in Figure 6.

The scheme that demonstrates characteristic fabrication parameters and 2PA cross-section of the synthesized and reference compounds is shown in Figure 7. The power between lower polymerization threshold and higher burning threshold is defined as the fabrication window (FW). It is preferable to have a broad and shifted FW to the lower energies. This may lead to high throughput in mass production because this could allow splitting the initial laser beam for parallel processing, while optical damage of the material can be avoided at high laser powers.

From Figure 7 a clear relationship can be seen between 2PA cross-section and FW for the reference and **4a**, **4b**, and **6a** compounds. FWs tend to be broader as the 2PA cross-section is increasing. Only compound **6b**, which exhibits the highest 2PA cross-section, had the narrowest FW. This is most probably related to the lower photoinitiation efficiency, which can be influenced by optimal conformation of compound **6b**, which in turn might be related to the presence of methyl group on the cyclohexane ring.

Preosteoblastic Cell Adhesion. Representative optical microscopy images (Figure 8) show the morphology of preosteoblastic cells cultured on various material surfaces and on the polystyrene control surface for 1, 3, and 7 days at a 10-fold magnification. Cells seeded for 1 day in culture indicate a

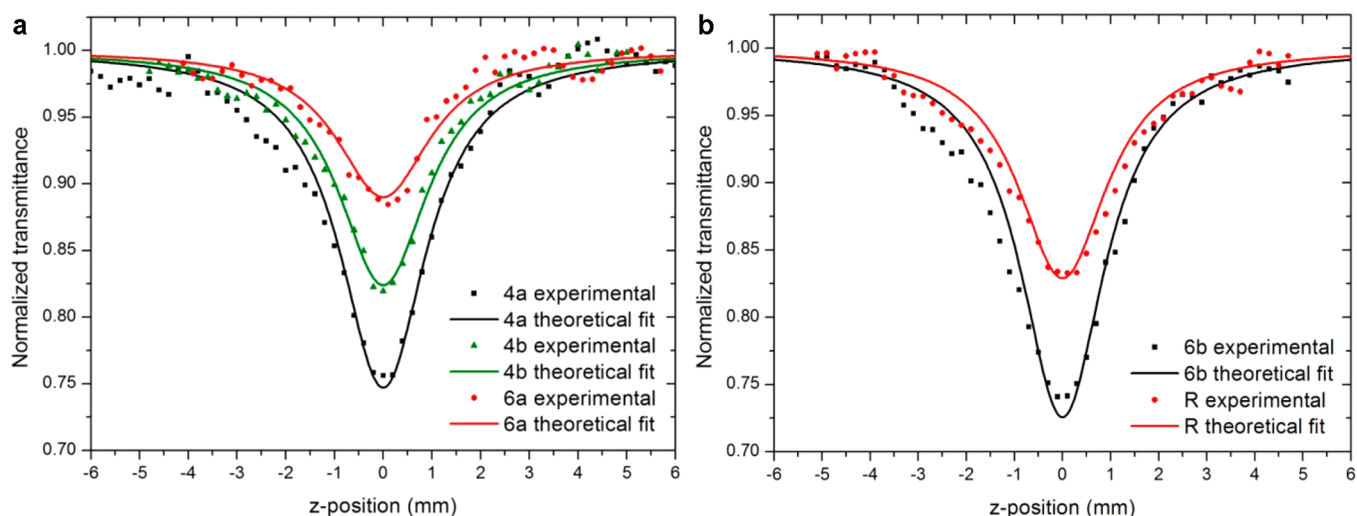


Figure 5. Data of z-scan measurements of 2PA in compounds. (a) Compounds **4a**, **4b**, and **6a** at the same level of laser intensity (200 GW/cm^2) and concentration (0.01 M); (b) **6b** (87 GW/cm^2 , 0.01 M) and **R** (115 GW/cm^2 , 0.25 M).

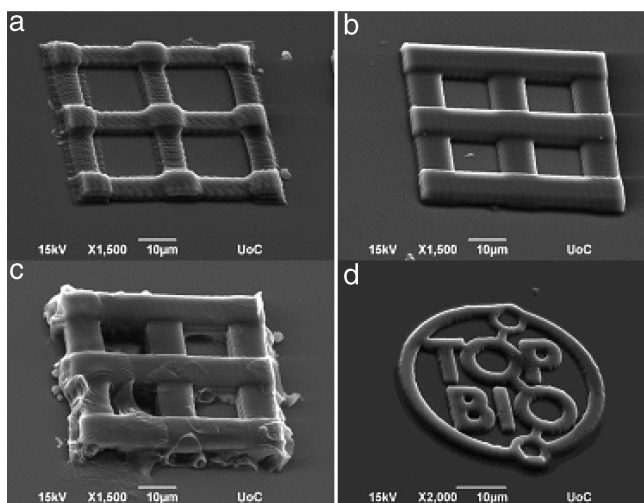


Figure 6. Typical microstructures fabricated under three different conditions using compound **6b** as initiator: (a) polymerization threshold, (b) good structuring threshold, (c) burning threshold, and (d) logo of EU ITN funding this research.

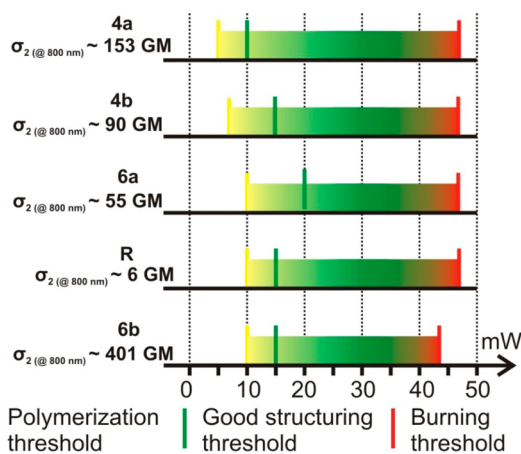


Figure 7. 2PA cross-sections, fabrication window, and threshold values of the compounds.

similar spindle-shaped morphology among the different film surfaces made from the compounds **4b**, **6a**, **6b**, and **4a**, which is comparable to that on the polystyrene control surface (Figure 8, top panel). After 3 days in culture, cells displayed a similar elongated morphology and number on all examined surfaces, indicating a comparable growth rate (Figure 8, middle panel). After 7 days in culture, a clear proliferation increase was observed with a dense layer of well-spread flattened cells completely covering all material surfaces, as shown in the bottom panel of Figure 8.

Cell Viability and Proliferation. Figure 9 shows the results from the investigation of the preosteoblastic cells' viability on PLA films performed using the PrestoBlue assay after 1, 3, and 7 days in culture. We performed the cytocompatibility investigations on geometrically well-defined films in order to quantify the cell proliferation results. For all examined materials we observed a strong initial cell adhesion and a subsequent cell proliferation increase after 3 and 7 days. The cell number on the different material films increased two times from day 1 to day 3 and three times from day 1 to day 7. The cell viability was up to 100% compared to the tissue culture treated polystyrene surface for all six materials at the three investigated time points. The results indicate the absence of any cytotoxic effects and suggest that all six examined materials are biocompatible and thus can be used for the fabrication of biomaterial scaffolds.

CONCLUSIONS

In summary, we provided a synthetic entry to novel two-photon photoinitiators with donor–acceptor–donor (D–A–D) structure. We have demonstrated that for π -expanded coumarin dyes maximum values of $\sigma_2 \approx 400 \text{ GM}$ in the near-IR range of wavelengths can be reached. The introduction of peripheral dialkylamino groups proved to be an excellent strategy to achieve at the same time good solubility of π -expanded coumarins and strong charge-transfer character. As a result, a very broad fabrication window has been achieved in direct laser writing ($10\text{--}15\text{--}40\text{--}45 \text{ mW}$), which favorably compare with previous TPIP initiators.^{33,35,37,38,52} The other notable findings are as follows: (a) A detailed study of the photophysical properties of the products and their simpler models allowed us to determine that replacing the cyclopentanone unit with a 4-

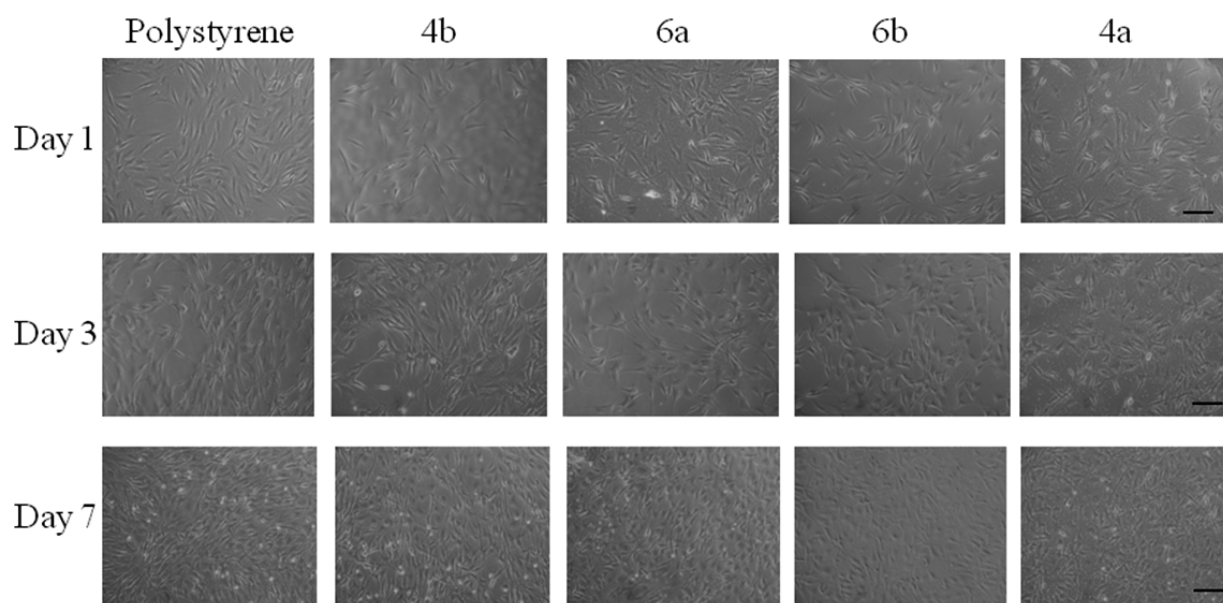


Figure 8. Optical microscopy images of preosteoblastic cells seeded on polystyrene and custom-made photoinitiator **4b**, **6a**, **6b**, and **4a** film surfaces after 1 day (top panel), 3 days (middle panel), and 7 days (bottom panel). Scale bar represents 50 μm .

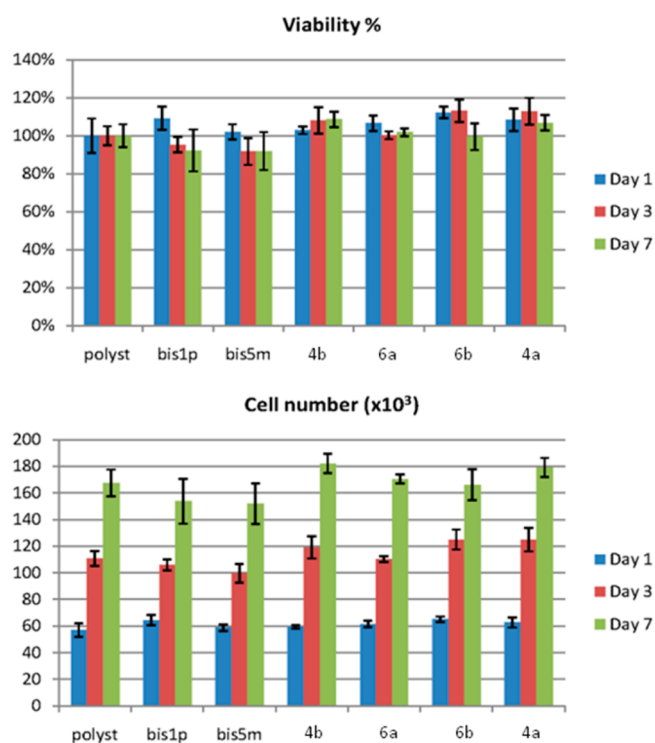


Figure 9. MC3T3-E1 cell viability on six different material surfaces related to the tissue culture treated polystyrene control (top graph), and proliferation expressed in cell numbers after 3 and 7 days in culture (bottom graph). Values represent averages of triplicates with standard deviations.

methylcyclohexanone unit leads to an increase in the 2PA cross-section while bathochromically shifting the absorption band and decreasing the luminescence quantum yield; (b) bis-coumarins display lifetimes of the order of tens of picoseconds; (c) bis-coumarin possessing the highest two-photon absorption cross-section is not the best overall performer, which emphasizes the critical influence of radical photoinitiation ability; (d) our results indicate a strong preosteoblastic cell

adhesion on the different material surfaces from the first day and up to 3 and 7 days in culture, exhibiting characteristic spindle-shaped morphology comparable with that observed on the polystyrene control surface; (e) additionally, a proliferation increase after 3 and 7 days in culture reflects the absence of any cytotoxic effect and thus the biocompatibility of these materials.

■ ASSOCIATED CONTENT

📄 Supporting Information

¹H NMR and ¹³C NMR spectra of all new compounds, absorption (in TOL and DCM) and excitation spectra in TOL; prompt and delayed luminescence measured in TOL glassy solutions at 77 K for compounds **4a** and **4b**. This material is available free of charge via the Internet at <http://pubs.acs.org>.

■ AUTHOR INFORMATION

Corresponding Authors

*(L.F.) Fax: +39 (0)51 639 98 44. E-mail: lucia.flamigni@isof.cnr.it.

*(M.F.) Fax: 0030 2810 391318. E-mail: mfarsari@iesl.forth.gr.

*(D. T. G.) Fax: 0048 22 6326681. E-mail: dtgryko@icho.edu.pl.

Author Contributions

The manuscript was written through contributions of all authors. All authors have given approval to the final version of the manuscript.

Notes

The authors declare no competing financial interest.

#Mr. Paulius Danilevicius passed away unexpectedly on September 10, 2013.

■ ACKNOWLEDGMENTS

The research leading to these results has received funding from the European Community's Seventh Framework Marie Curie ITN program TopBio (PITN-GA-2010-264362). We thank Jillian Larsen for amending the manuscript.

REFERENCES

- (1) Maruo, S.; Nakamura, O.; Kawata, S. *Opt. Lett.* **1997**, *22*, 132.
- (2) Radke, A.; Gissibl, T.; Klotzbucher, T.; Braun, P. V.; Giessen, H. *Adv. Mater.* **2011**, *23*, 3018–3021.
- (3) Vasilantonakis, N.; Terzaki, K.; Sakellari, I.; Purlys, V.; Gray, D.; Soukoulis, C. M.; Vamvakaki, M.; Kafesaki, M.; Farsari, M. *Adv. Mater.* **2012**, *24*, 1101–1105.
- (4) Chen, Y.-S.; Tal, A.; Kuebler, S. M. *Chem. Mater.* **2007**, *19*, 3858–3860.
- (5) Gansel, J. K.; Thiel, M.; Rill, M. S.; Decker, M.; Bade, K.; Saile, V.; von Freymann, G.; Linden, S.; Wegener, M. *Science* **2009**, *325*, 1513–1515.
- (6) Raimondi, M. T.; Eaton, S. M.; Lagana, M.; Aprile, V.; Nava, M. M.; Cerullo, G.; Osellame, R. *Acta Biomater.* **2013**, *9*, 4579–4584.
- (7) Albota, M.; Beljonne, D.; Bredas, J. L.; Ehrlich, J. E.; Fu, J. Y.; Heikal, A. A.; Hess, S. E.; Kogej, T.; Levin, M. D.; Marder, S. R.; Maughon, D. M.; Perry, J. W.; Rumi, M.; Subramaniam, G.; Webb, W. W.; Li, X.; Xu, C. *Science* **1998**, *281*, 1653–1656.
- (8) Chung, S. J.; Kim, K. S.; Lin, T. C.; He, G. S.; Swiatkiewicz, J.; Prasad, P. N. *J. Phys. Chem. B* **1999**, *103*, 10741–10745.
- (9) Belfield, K. D.; Morales, A. R.; Hales, J. M.; Hagan, D. J.; Van Stryland, E. W.; Chapela, V. M.; Percino. *Chem. Mater.* **2004**, *16*, 2267–2273.
- (10) Belfield, K. D.; Ren, X. B.; Van Stryland, E. W.; Hagan, D. J.; Dubikovskiy, V.; Miesak, E. J. *J. Am. Chem. Soc.* **2000**, *122*, 1217–1218.
- (11) Belfield, K. D.; Schafer, K. J.; Liu, Y. U.; Liu, J.; Ren, X. B.; Van Stryland, E. W. *J. Phys. Org. Chem.* **2000**, *13*, 837–849.
- (12) Schafer, K. J.; Hales, J. M.; Balu, M.; Belfield, K. D.; Van Stryland, E. W.; Hagan, D. J. *J. Photochem. Photobiol., A* **2004**, *162*, 497–502.
- (13) Telitel, S.; Lalevée, J.; Blanchard, N.; Kavalli, T.; Tehfe, M. A.; Schweizer, S.; Morlet-Savary, F.; Graff, B.; Fouassier, J. P. *Macromolecules* **2012**, *45*, 6864–6868.
- (14) Tehfe, M. A.; Dumur, F.; Graff, B.; Morlet-Savary, F.; Fouassier, J. P.; Gignes, D.; Lalevée, J. *Macromolecules* **2012**, *45*, 8639–8647.
- (15) Telitel, S.; Schweizer, S.; Morlet-Savary, F.; Graff, B.; Tschamber, T.; Blanchard, N.; Fouassier, J. P.; Lelli, M.; Lacôte, E.; Lalevée, J. *Macromolecules* **2013**, *46*, 43–48.
- (16) Tehfe, M. A.; Dumur, F.; Graff, B.; Clément, J. L.; Gignes, D.; Morlet-Savary, F.; Fouassier, J. P.; Lalevée, J. *Macromolecules* **2013**, *46*, 736–746.
- (17) Davy-Louis Versace, D. L.; Dalmas, F.; Fouassier, J. P.; Lalevée, J. *ACS Macro Lett.* **2013**, *2*, 341–345.
- (18) Tehfe, M. A.; Dumur, F.; Graff, B.; Gignes, D.; Fouassier, J. P.; Lalevée, J. *Macromolecules* **2013**, *46*, 3332–3341.
- (19) Tehfe, M. A.; Dumur, F.; Graff, B.; Morlet-Savary, F.; Fouassier, J. P.; Gignes, D.; Lalevée, J. *Macromolecules* **2013**, *46*, 3761–3770.
- (20) Xiao, P.; Dumur, F.; Tuan Bui, T.; Goubard, F.; Graff, B.; Morlet-Savary, F.; Fouassier, J. P.; Gignes, D.; Lalevée, J. *ACS Macro Lett.* **2013**, *2*, 736–740.
- (21) Xiao, P.; Dumur, F.; Thirion, D.; Fagour, S.; Vacher, A.; Sallenave, X.; Morlet-Savary, F.; Graff, B.; Fouassier, J. P.; Gignes, D.; Lalevée, J. *Macromolecules* **2013**, *46*, 6786–6793.
- (22) Xiao, P.; Dumur, F.; Graff, B.; Gignes, D.; Fouassier, J. P.; Lalevée, J. *Macromolecules* **2013**, *46*, 7661–7667.
- (23) Xiao, P.; Dumur, F.; Graff, B.; Morlet-Savary, F.; Vidal, L.; Gignes, D.; Fouassier, J. P.; Lalevée, J. *Macromolecules* **2014**, *47*, 26–34.
- (24) Xiao, P.; Dumur, F.; Graff, B.; Gignes, D.; Fouassier, J. P.; Lalevée, J. *Macromolecules* **2014**, *47*, 601–608.
- (25) Ibrahim, A.; Di Stefano, L.; Tarzi, O.; Tar, H.; Ley, C.; Allonas, X. *Photochem. Photobiol.* **2013**, *89*, 1283–1290.
- (26) Monroe, B. M.; Smothers, W. K.; Keys, D. E.; Krebs, R. R.; Mickish, D. J.; Harrington, A. F.; Schicker, S. R.; Armstrong, M. K.; Chan, D. M. T.; Weathers, C. I. *J. Imaging Sci.* **1991**, *35*, 19–25.
- (27) Jones, G.; Xuan, P. T.; Schwarz, W. *Tetrahedron Lett.* **1982**, *23*, 5505–5508.
- (28) Fouassier, J. P.; Wu, S. K. *J. Appl. Polym. Sci.* **1992**, *44*, 1779–1786.
- (29) Specht, D. P.; Martic, P. A.; Farid, S. *Tetrahedron.* **1982**, *38*, 1203–1211.
- (30) von Freymann, G.; Ledermann, A.; Thiel, M.; Staude, I.; Essig, S.; Busch, K.; Wegener, M. *Adv. Funct. Mater.* **2010**, *20*, 1038–1052.
- (31) Hao, F.; Liu, Z.; Zhang, M.; Liu, J.; Zhang, S.; Wu, J.; Zhou, H.; Tian, Y. *Spectrochimica Acta, Part A* **2014**, *118*, 538–542.
- (32) Li, Z.; Pucher, N.; Cicha, K.; Torgensen, J.; Ligon, S. C.; Ajami, A.; Husinsky, W.; Rosspeintner, A.; Vauthey, E.; Naumov, S.; Scherzer, T.; Stampfl, J.; Liska, R. *Macromolecules* **2013**, *46*, 352–361.
- (33) Pucher, N.; Rosspeintner, A.; Satzinger, V.; Schmidt, V.; Gescheidt, G.; Stampfl, J.; Liska, R. *Macromolecules* **2009**, *42*, 6519–6528.
- (34) Lu, W.-E.; Dong, X.-Z.; Chen, W.-Q.; Zhao, Z.-S.; Duan, X.-M. *J. Mater. Chem.* **2011**, *21*, 5650–5659.
- (35) LaFratta, C. N.; Fourkas, J. T.; Baldacchini, T.; Farrer, R. A. *Angew. Chem., Int. Ed.* **2007**, *46*, 6238–6258.
- (36) Xue, J. Q.; Zhao, Y. X.; Wu, J.; Wu, F. P. *J. Photochem. Photobiol. A: Chem.* **2008**, *195*, 261–266.
- (37) Xue, J.; Zhao, Y.; Wu, F. *J. Phys. Chem. A* **2010**, *114*, 5171–5179.
- (38) Wang, T.; Zhao, Y.; Shi, M.; Wu, F. *Dyes Pigm.* **2007**, *75*, 104–110.
- (39) Feng, J. G.; Arai, C.; Kaiser, M.; Wittlin, S.; Brun, R.; Ihara, M. *J. Med. Chem.* **2008**, *51*, 3654–3658.
- (40) James, W.; Andrew, M.; Peter, K.; Erwin, B. *Can. J. Chem.* **1999**, *77*, 903–912.
- (41) Ovsianikov, A.; Viertl, J.; Chichkov, B.; Oubaha, M.; MacCraith, B.; Sakellari, I.; Giakoumaki, A.; Gray, D.; Vamvakaki, M.; Farsari, M.; Fotakis, C. *ACS Nano* **2008**, *2*, 2257–2262.
- (42) Rurak, K.; Spieles, M. *Anal. Chem.* **2011**, *83*, 1232–1242.
- (43) Flamigni, L.; Talarico, A. M.; Serroni, S.; Puntoriero, F.; Gunter, M. J.; Johnston, M. R.; Jaynes, T. P. *Chem.—Eur. J.* **2003**, *11*, 2649–2659.
- (44) Nazir, R.; Danilevicius, P.; Gray, H.; Farsari, M.; Gryko, D. T. *Macromolecules* **2013**, *46*, 7239–7244.
- (45) Sakellari, I.; Kabouraki, E.; Gray, D.; Purlys, V.; Fotakis, C.; Pikulin, A.; Bityurin, N.; Vamvakaki, M.; Farsari, M. *ACS Nano* **2012**, *6*, 2302–2311.
- (46) Terzaki, K.; Kissamitaki, M.; Skarmoutsou, A.; Fotakis, C.; Charitidis, C. A.; Farsari, M. *J. Biomed. Mater. Res., Part A* **2013**, *101A*, 2283–2294.
- (47) An, L. T.; Zou, J. P.; Zhang, L. L. *Catal. Commun.* **2008**, *9*, 349–354.
- (48) Watanabe, K.; Imazawa, A. *Bull. Chem. Soc. Jpn.* **1982**, *55*, 3208–3211.
- (49) Ryan Davis, R.; Das, U.; Mackay, H.; Brown, T.; Mooberry, S. L.; Dimmock, J. R.; Lee, M.; Pati, H. *Arch. Pharm. Chem. Life Sci.* **2008**, *341*, 440–445.
- (50) Tasiar, M.; Gryko, D. T.; Pielacińska, D.; Zanelli, A.; Flamigni, L. *Chem.—Asian J.* **2010**, *5*, 130–140.
- (51) For biexponential decays, the radiative rate constant $k_{\text{rad}} = \phi_{\text{R}}/\tau$ is calculated for the major component.
- (52) Ligon, S. C.; Husár, B.; Wutzel, H.; Holman, R.; Liska, R. *Chem. Rev.* **2014**, *114*, 557–589.